Kingdom of Saudi Arabia

Al-Imam Muhammed Ibn Saud Islamic University

College of Sciences

Chemistry departement

المملكة العربية السعودية

جامعة الإمام محمد بن سعود الإسلامية

كلية العلوم

قسم الكيمياء

بسم الله الرحمن الرحيم

Synthesis, characterization of pure and nonmetal doped ZnO nanoparticles and their applications

A graduation research project

Submitted to

Chemistry Department in Partial Fulfillment of the Requirements for the Completion of the Degree of Bachelor of Science in Chemistry

By

Abdel rahman Mohamed Mohamed Al Shehry

Under supervision

By

Dr. Mohamed Khairy Abdel Fattah

Second Semester, May 2016

Content

الملخص

الهدف من هذا المشروع اولا تحضيرجسيمات نانومترية من اكسيد الزنك النقي واكسيد الزنك المطعم بلافلز مثل النيتروجين والكبريت بواسطة طريقة الترسيب في وجود دعامة (Tween 80). ثانيا التعرف علي شكل وحجم الجسيمات عن طريق الميكروسكوب الالكترونى الماسح و التعرف علي التركيب البلوري بواسطة جهاز قياس حيود الاشعة السينية. ثالثا دراسة تأثير عملية التطعيم في تحسين الخواص الضوئية وقدرة الادمصاص لصبغة الميثلين الازرق. وقد تم تحضير عينات حجم جسيماتها تتراوح مابين ٢١ الي ٣١ نانومتر. ووجد ان عملية التطعيم قد حسنت في خواص اكسيد الزنك الضوئية وتحسين قدرته علي امتصاص الضوء المرئي. ووجد ان العينات لها قدرة علي امتزاز صبغة الميثلين الازرق ونتائج عملية الامتزاز تتفق مع نموذج فرندليش.

Abstract

The project aimed to synthesized nano-crystalline ZnO and non metal doped ZnO particles using precipitation method in presence of template (Tween 80). Characterization of samples by scanning electron microscopy (SEM) and X-ray diffraction (XRD) was studied. The effect of doping process on optical properties and adsorption performance have been studied and discussed. The results show the nano-crystalline ZnO, N and S doped ZnO particles were synthesized using template method with particle diameter ranged from 21 to 31 nm. The samples well characterized with different techniques. The doping process enhanced the absorption of visible light. Moreover, The equilibrium data of adsorption are in good agreement with the Freundlich isotherm model. The samples show effective adsorption at short time 55 min.

1. Introduction

Nanoparticles and nanostructural materials represent an evolving technology that has an impact on an incredibly wide number of industry and markets. Nanotechnology deals with the synthesis of materials, structures and/or devices having dimensions up to ~ 100 nm with new properties. The synthesis and characterization of nanocrystals is a very exciting emerging field of research which has received important scientific and technological attention [1]. A variety of supermolecular ensembles, multifunctional supermolecules, carbon nanotubes, metal and semiconductor nanoparticles[1], have been synthesized and proposed as potential building blocks of optical and electronic devices.

1.1. Synthesis of Nanostructured Materials

In general, there are two approaches to nanoparticle production that are commonly referred to as ‘top-down’ and ‘bottom-up’. ‘Top-down’ nanoparticles are generated from the size reduction of bulk materials. They generally rely on physical, the combination of physical and chemical, electrical or thermal processes for their production. Such methods include high-energy milling, mechano-chemical processing, electro-explosion, laser ablation, sputtering and vapour condensation.

'Bottom-up' approaches generate nanoparticles from the atomic or molecular level and thus are predominantly chemical processes (Fig.1). Commonly used techniques are crystallisation/precipitation, sol gel methods, chemical vapour deposition and self-assembly routes. Some processes may use a combination of both.

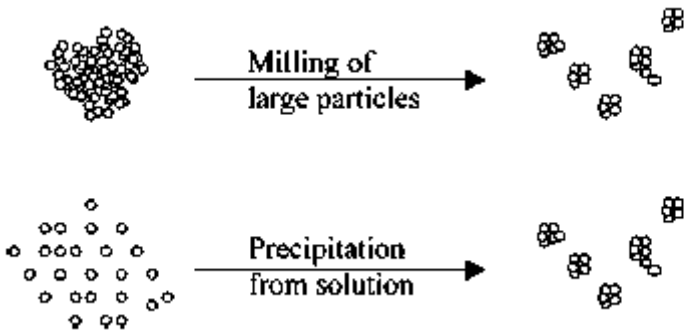

Fig. 1: Schematic of the two general nanoparticle production techniques.

Both approaches may be performed in all three states of matter, i.e., vapour, solid or liquid (or combination of these) and the limits to the physical size of nanoparticles produced by either approach are converging and may overlap.

The choice of particle size, from a product design perspective, is directly influenced by process economics, capability to supply and the adequacy and type of performance required in the target application. Nanoparticles have a size dimension up to 100 nm and thus represent a 'bridge' between the quantum and 'real' world (micro and macro). Table 1 summarizes the range of production processes by type.

Table 1: Summary of production processes by type.

Process routes	
Top-down	Bottom-up
High-energy milling Chemical mechanical milling Vapour phase condensation Electro-explosion Laser ablation Sputtering	Crystallisation Sol-gel Chemical vapour deposition Self-assembly

1.2. Properties of Nanostructured Materials

Nanomaterial properties differ from their ‘real’ (bulk) counterparts primarily due to changes in physical attributes (size, shape and specific surface area) and quantum effects such as quantum confinement (the organization of energy levels into which electrons can climb or fall being squeezed into a dimension that approaches a critical quantum measurement). As a result of these nanoscale particle dimensions the properties that can change from those observed in the bulk include mechanical, physical, chemical, electronic, optical and magnetic. A change in more than one property may occur in the same particle (e.g. optical and electrical) so that particles with a range of functionalities can be engineered for target applications. Moreover, these properties may be used intentionally to directly affect bulk properties of any material system into which they are incorporated. Some examples of property changes resulting from nanoparticle dimensionality are presented below:

a) Surface activity: when the particle size of Au, for example, is reduced to 2–10 nm the catalytic activity of supported gold catalysts can be significantly enhanced [2].

b) Mechanical: the hardness of silicon nanospheres (20–50 nm) has been measured to be four times greater than the expected value for bulk silicon (50 Gpa cf. 12 Gpa) [3].

c) Optical: nanoparticles, with dimensions less than the wavelength of light (400–700 nm), appear transparent when well dispersed. Moreover, colour and luminescent properties can be significantly altered [1].

d) Electronic: the electronic structure of a nanocrystal critically depends on its size. For small particles, the electronic energy levels are not continuous as in bulk materials, but discrete, due to the confinement of the electron wavefunction as a result of the physical dimensions of the individual nanoparticles. This confinement exhibits quantum size effects influencing properties such as electrical conductivity and magnetic susceptibility. Perhaps the most impressive example of the relationship between size and electronic

e) Magnetic: magnetic properties of nanoparticles of transition metals such as Co, Ni show marked variations with size [4].

As a particle becomes smaller it theoretically can physically fit into, be assembled or positioned onto/into or pass through significantly smaller spaces. The implications of this feature are enormous in terms of the potential applications.

Perhaps the greatest realised impact of this has been in the functional quality and performance properties of bulk material systems such as polymer nanocomposites and coatings (lighter, stronger, functionally smarter); ceramic composite materials (improved fracture toughness, wear resistance, greater biocompatibility, etc.); data storage and processing systems (greater capacity to store and process at reduced size); dispersions (for chemical mechanical polishing, personal care); sensors and instrumentation, drug delivery systems and enhanced activity in catalytic processes.

1.3. Applications of Nanostructured Materials

Nanostructured materials exhibit a host of interesting new phenomena directly related to their reduced dimensionality. Not only the electronic, magnetic and optical properties but also chemical, electrochemical and catalytic properties of nanostructured materials are very different from those of the bulk form and depend sensitively on size, shape and composition [5]. The large surface-to-volume ratio and the variation in geometry and electronic structure have a dramatic effect on transport and catalytic properties. The range of applications is broad and growing with the current main uses as functional additives or precursors for emulsions, composites and coatings. Recently, much interest has been focused on semiconductor nanocrystals because they exhibit strongly size-dependent optical and electrical properties.

1.4. Waste water treatment

Nowadays, the circulation of water in industrial production process is recognized as a necessity. There are new challenges concerning the treatment of raw water as well. The pollution of the past now affects natural water sources, surface waters, and ground water [6].

The main causes of surface and groundwater contamination are industrial effluents (even in small amounts), excessive use of pesticides, fertilizers (agrochemicals) and domestic waste landfills. Wastewater (WW) treatment is usually based on physical and biological processes. After elimination of particles in suspension, the usual process is biological treatment (natural decontamination). Unfortunately, some organic pollutants, classified as bio-recalcitrant, are not biodegradable.

Azo dyes are broadly used in the textile industry, and also widely employed to color solvents, inks, paints, varnishes, paper, plastic, rubber, foods, drugs, and cosmetics. More than two thousand azo dyes are known and over half of the commercial dyestuffs are azo dyes [7]. The manufacturing of azo dyes and their application produce wastewater contaminated with azo dyes [8], which are discharged through conventional wastewater treatment plants. Unfortunately, the activated sludge process dose not decomposes most azo dyes, causing a potentially serious disposal problem [9]. Some azo dyes and their dye precursors have been shown to be or are suspected to be human carcinogens [10]. Therefore, studying the destruction of azo dyes in wastewater treatment processes is of utmost importance. Consequently, alternative technologies which can decompose the nonbiodegradable azo dyes have to be explored.

In general, dye wastewater can be treated by adsorption onto activated carbon or by coagulant. Those treatment methods mainly transfer the contaminant from wastewater to solid waste. Therefore, further disposal of sludge is needed for adsorption and coagulation processes [11].

According to the literature, semiconductor photochemistry continues to be the hottest subject in photochemistry. Recently, greatest interest in the subject has focused primarily on the semiconductor photocatalysis (SPC) as a possible route for providing cleanwater, air and surfaces [12].

Recently, considerable amount of waste water with color has been generated from many industries including textile, leather, paper, printing, dyestuff, plastic and so on. Removal of dye materials from contaminated water is very important because water quality is highly influenced by color and even a small amount of dye is highly visible and undesirable. Moreover, many dyes are considered to be toxic and even carcinogenic [13]. It is difficult to degrade dye materials because they are very stable to light and oxidation reactions [13].

Dye toxic waste in aquatic environments remains nowadays a real problem. Wide variety of dyes are extensively used in different industries, such as food industries, paper, leather, textile, cosmetic, paper, etc.. Different techniques, such as ozonation, oxidation, ion exchange, coagulation, flocculation membrane filtration, biodegradation, precipitation, photocatalysis and adsorption are used as a simple and cost effective technique for the removal of dyes [13–19]. Among the proposed systems, removal of dyes by adsorption innovations is viewed as one of the competing

techniques due to high productivity, financial practicality and effortlessness of configuration/operation [13, 14]. Several adsorbents have been utilized for the removal of dyes like, activated charcoal [20], clay[21], agriculture waste or polymers [22]. Nowadays conducting polymer, polyaniline, is used as adsorbent for the removal of dyes and heavy metal [23]. Cerium nanoparticles have been used in a variety of industrial applications such as catalysis, solar energy devices, optical display technology and corrosion prevention [24].

Adsorption is a well-known equilibrium separation process and an effective method for water decontamination applications. Adsorption has been found to be superior to other techniques for water re-use in terms of initial cost, flexibility and simplicity of design, ease of operation and insensitivity to toxic pollutants. Adsorption also does not result in the formation of harmful substances. Adsorption occurs in three steps. First step, the adsorbate diffuses from the major body of the stream to the external surface of the adsorbent particle. Second step, the adsorbate migrates from the relatively small area of the external surface to the pores within each adsorbent particle. The bulk of adsorption usually occurs in these pores because there is the majority of available surface area. Final step, the contaminant molecule adheres to the surface in the pore.

1.5. Zinc Oxide

1.5.1. Crystal structure

Zinc oxide normally occurs in the hexagonal wurtzite structure as shown in Fig. 2 [25]. can be transformed to the cubic rocksalt (NaCl) structure by the application of high pressure. This cubic phase has been reported to be metastable at atmospheric pressure. ZnO has many attractive properties, such as the direct wide bandgap (3.37 eV), large exciton binding energy (60 meV at room temperature), good piezoelectric characteristics, chemical stability and biocompatibility. These properties suggest a host of possible practical applications, notably in the area of ultraviolet/blue emission devices [26].

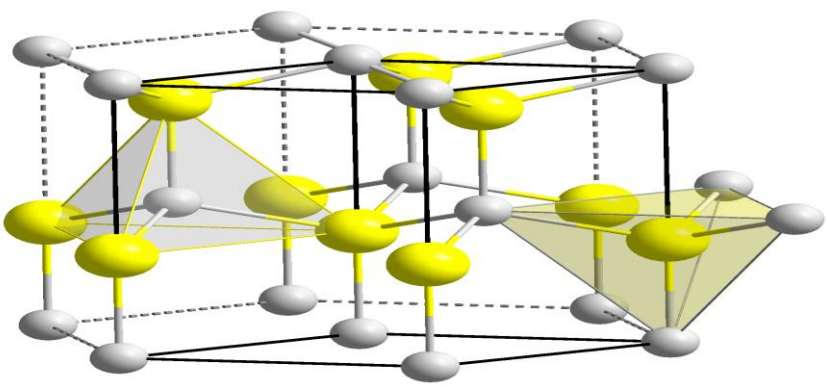

Fig. 2: hexagonal wurtzite structure of ZnO.

1.5.2. Applications

ZnO has interesting and wide applications in ceramics, catalysis, rubber, cosmetics, varistors, ect. The size, morphology and charge of ZnO particles play an important role in these applications. Nanosize ZnO particles are efficient in killing many bacteria. Thin films or nanoscale coating of ZnO nanoparticles on suitable substrates is also important for its potential applications as substrates for functional coatings, printing, UV inks, e-print, optical communications (security papers), protection, barriers, portable energy, sensors, photocatalytic wall paper with antibacterial activity etc [27].

1.5.3. Nonmetal doped ZnO

Recently, some groups have demonstrated that C, S or N impurity can modify the electronic structure and optical properties of the intrinsic ZnO efficiently [28–32].

The visible light absorption require band gap narrowing of ZnO. Band gap narrowing through ZnO doping can be achieved by three main approaches, i) the elevation of the valence band maximum, ii) lowering of the conduction band minimum and iii) introduction of localized energy levels within the band gap [33]. Fig. 3 illustrates the three different situations for achieving visible light absorption of ZnO by metal and nonmetal doping [34].

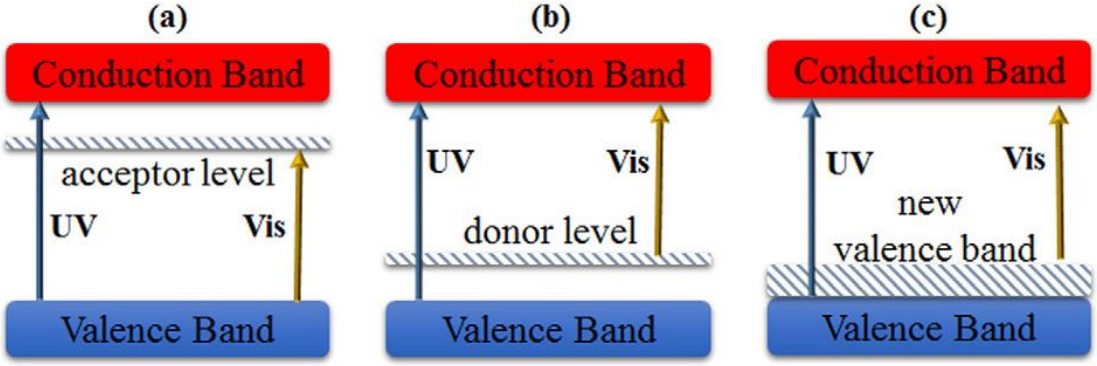

Fig. 3. Schematic representation of the doped ZnO energy levels: (a) acceptor level and (b) donor level with metal doping, (c) new valence band formation by nonmetal doping. (a, b, c) Reproduced with permission from [34]. Copyright 2010 American Chemical Society.

In the nonmetal doping case, as depicted in Fig. 3(c), doping creates a new valence band state that leads to band gap narrowing by elevating the valence band maximum. Therefore, unlike metal doping, nonmetal doping is less likely to form recombination centers. Thus, nonmetal doping is more effective to improve the absorption of visible light as well as the photocatalytic activity of ZnO under visible light [33, 34, 35].

1.5.3.1. S-doped ZnO

Due to the larger Bohr radius of the S atom than O and the difference in their electronegativity, it is suggested that sulfur doping of ZnO can modify its optical, electrical and photocatalytic properties. They reported that the physical properties of S-doped ZnO are influenced by the different substitutional sites of S in ZnO lattice. For SO-doped ZnO, the S 3p states are located above the valence band and mix with O 2p states which result in band gap narrowing [36].

1.5.4.2. N-doped ZnO

Until now, among all nonmetal dopants, nitrogen has attracted the most attention. This is due to its advantages, including the similarity of nitrogen and oxygen ionic radii, N2p and O2p energy states, high solubility, and also low formation energy. Hybridization of N 2p and O 2p states raises the valence band upper edge and thus, band gap narrowing occurs [37–39]. Fig. 4(a) shows the two main routes of nitrogen doping in ZnO structure, including the replacement of oxygen by nitrogen (substitutional sites) or occupation of interstitial sites [40, 41]. Nitrogen dopant causes formation of oxygen vacancies and Zn interstitials during doping, which creates an appropriate electronic structure for band gap narrowing.

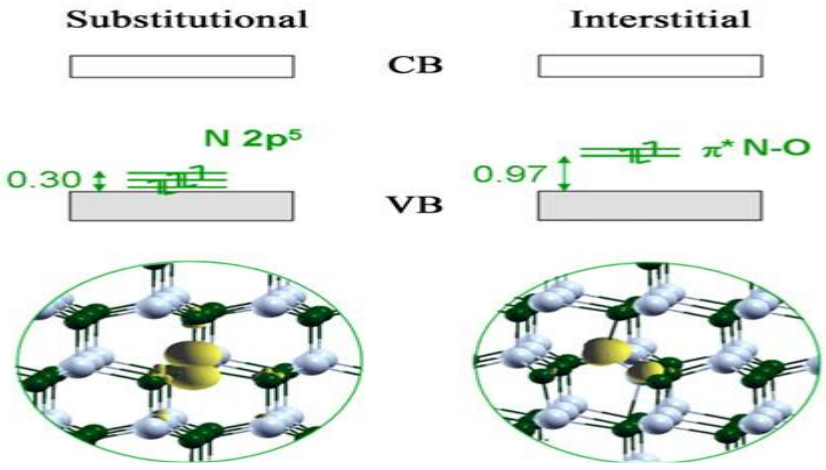

Fig. 4: Schematic representation of the Kohn–Sham levels in the band gap of the N-doped ZnO (top) and ball-and-stick representation (bottom) with spin density plot (yellow) for substitutional (left) and interstitial doping (right).

1.6. Literature survey

X. Xie et. al. [42] reported that the S-doped ZnO was prepared by new ecofriendly method, which involves simple mechanochemical synthesis followed by thermal decomposition of bisthiourea zinc oxalate (BTZO) powders. The BTZO was characterized by FTIR and TG–DTA analysis while S-doped ZnO crystallite was characterized by XRD, XPS, SEM, EDXS, and photoluminescence (PL) spectra. X-ray diffraction data suggest the single phase wurtzite structure for S-doped ZnO and the incorporation of sulfur expand the lattice constants of ZnO. Room temperature PL spectra show more number of oxygen vacancies in S-doped ZnO as compare to that of pure ZnO. Photocatalytic activity of S-doped ZnO was checked by means of solar photocatalytic degradation (PCD) of resorcinol, using a batch photoreactor. The PCD efficiency of S-doped ZnO was found to be 2 times greater than that of pure ZnO. The inherent relationship between PL intensity and photocatalytic activity of S-doped ZnO was discussed.

S-doped ZnO nanoparticles (S-ZnO) were synthesized via a one-step and green method [43]. In this method, zinc acetate dihydrate was used as a precursor and sulfur was the dopant. The reaction between zinc salt and S occurred in PEG200 media. X-ray diffraction, field emission scanning electron microscopy, transmission electron microscopy, high-resolution transmission electron microscopy, energy-dispersive X-ray spectroscopy, Fourier transform infrared spectroscopy, UV–Vis

spectroscopy and room temperature photoluminescence were used to characterize the products. The results show that the molar ratio of Zn(II) and S determines the composition, structure, surface morphology, and luminescence properties of the products greatly. When the number of moles of sulfur (nS) is smaller than that of zinc salt (nZn), the products are S-ZnO with diameters of 40–55 nm and they have ultraviolet absorption peaks at 363 nm. The incorporation of S into ZnO is supported by broadening and lower Bragg angle shift in XRD pattern. FTIR spectra show that PEG200 adsorbs onto the surfaces of the S-ZnO as a capping agent. PL spectra show that the effective sulfur doping enhances the green emission and suppresses the near band gap emission. The possible reaction and growth mechanism is also developed.

B-doped ZnO and N-doped ZnO powders have been synthesized by mechanochemical method and characterized by TG–DTA, XRD, SEM–EDX, XPS, UV–visible and photoluminescence (PL) spectra [44]. X-ray diffraction data suggests the hexagonal wurtzite structure for modified ZnO crystallites and the incorporation of nonmetal expands the lattice constants of ZnO. The room temperature PL spectra suggest more number of oxygen vacancies exist in nonmetal-doped ZnO than that of undoped zinc oxide. XPS analysis shows the substitution of some of the O atoms of ZnO by nonmetal atoms. Solar photocatalytic activity of B-doped ZnO, N-doped ZnO and undoped ZnO was compared by means of oxidative photocatalytic degradation (PCD) of Bisphenol A (BPA). B-doped ZnO showed better solar PCD efficiency as compare to N-doped ZnO and undoped ZnO. The PCD of BPA follows first order reaction kinetics. The detail mechanism of PCD of Bisphenol A was proposed with the identification of intermediates such as hydroquinone, benzene-1,2,4-triol and 4-(2-hydroxypropan-2-yl) phenol.

1.7. Aim of work

The purpose of the work is the improving optical absorption and raising the performance of ZnO to remove undesirable dyes in water by doping with non metals such as N and S. Studying the adsorption capability of samples to remove the dye and studying the suitable adsorption isotherms

2. Experimental Work

2.1. Materials

All chemical reagents were analytical grade and were used without further purification. The materials which used in our preparations are; zinc acetate ($Zn(CH_3COO)_2.2H_2O$), oxalic acid ($H_2C_2O_4.2H_2O$), urea, thiourea, Tween 80 and methylene blue MB all provided from Aldrich.

2.2. Synthesis of pure and doped ZnO nanoparticles

2.2.1. Synthesis of pure ZnO

0.15 M $H_2C_2O_4.2H_2O$ distilled water solution was slowly dropped into the mixture containing 0.1M $Zn(CH_3COO)_2.2H_2O$ in presence of Tween 80 surfactant as structure directing agent with constant stirring For 2 h. The precipitate obtained was filtered and washed with acetone for at least three times, dried at 120 ◦C. Finally, the copper doped ZnO sample was ignited at 450 ◦C for 2 h. The sample denoted as ZnO .

2-2.2. Synthesis of doped ZnO

0.15 M $H_2C_2O_4.2H_2O$ distilled water solution was slowly dropped into the mixture containing 0.1M $Zn(CH_3COO)_2.2H_2O$ and suitable amounts of urea or thiourea to synthesis 5% of N or S/ZnO in presence of Tween 80 surfactant as structure directing agent with constant stirring For 2 h. The precipitate obtained was filtered and

washed with acetone for at least three times, dried at 120 ◦C. Finally, the N or S doped ZnO sample was ignited at 450 ◦C for 2 h. The sample denoted as N/ZnO, S/ZnO.

2.3. Characterization methods

2.3.1. X-ray Diffraction (XRD)

The crystalline phases for all investigated samples were identified by X-ray diffraction (XRD) using a Diano (made by Diano Corporation, U.S.A.). The patterns were run with Cu-filtered CuKα radiation (λ = 1.5418Å) energized at 45 kV, and 10 mA. The samples were measured at room temperature in the range from 2θ = 10 to 80^{o}. The XRD phases present in the samples were identified with the help of ASTM Powder Data Files.

2.3.2. Scanning electron microscope (SEM)

Scanning electron microscopy (SEM), JEOL JEM-100CXII were taken to examine the morphology and dimension of the investigated samples using conductive carbon paint.

2.3.3. Optical properties

The optical absorption of the dye solution was measured in the range of 300 –800 nm with UV–vis spectrophotometer (Jasco V-550, Japan) using distilled water in the reference beam.

2.3.4. Adsorption studies

The adsorption of methylene blue dye (MB) from aqueous solution onto the adsorbents was performed using batch equilibrium technique. All the experiments were carried out at 25 °C. For the determination of adsorption isotherms, 25 mL of dye solution of known initial concentration was shaken with a certain amount of the adsorbent (15 mg) on a stirrer at 25 °C and pH = 7 for 55 min. Initial dye concentrations were changed in the range of 10 mg L^{-1} to 125 mg L^{-1}. Several beakers were placed on a multiposition magnetic stirrer and individually stirred at 400 rpm. After 24 h, samples were taken and allowed to settle and filtered. The concentration of the residual dye was measured using UV–vis spectrophotometer (Jasco V-550, Japan) at appropriate wavelength corresponding to the maximum absorption of MB dye (i.e., 665 nm). This data was used to calculate the adsorption capacity of the adsorbent. Initial dye concentration in the solution was varied to

investigate its effect on the adsorption capacity. The equilibrium adsorption capacities (qe) were then obtained by using the following mass balance equation.

$$q_e = (C_o - C_e)\frac{V}{W} \quad (1)$$

Where q_e is the adsorption capacity (dye adsorbed onto the mass unit of the sample, mg/g), Where C_o and C_e are the initial and equilibrium dye concentrations in solution (mg/L) respectively, W is the adsorbent amount (g), and V is the volume of solution (L). Adsorption isotherms were investigated by Langmuir and Freundlich models.

3. Theoretical review

3.1. Equilibrium adsorption isotherms

The equilibrium of adsorption is one of the critical physicochemical parts of the estimation relationship between the amount of adsorbate per unit of adsorbent (q_e) and its equilibrium solution concentration (C_e) at a constant-temperature and it is known as the adsorption isotherm. There are several isotherm models available for analyzing experimental sorption equilibrium parameters, the most common being the Langmuir and Freundlich models.

3.1.1. Langmuir model

The Langmuir adsorption [45] is based on the assumption that adsorption occurs at specific homogeneous sites within the adsorbent and once a dye molecule occupies a site, no further adsorption takes place at that site. Moreover, Langmuir's model of adsorption depends on the assumption of monolayer adsorption on a structurally homogeneous adsorbent, where all the sorption sites are identical and energetically equivalent. The intermolecular forces decrease rapidly with distance and can be used to predict the existence of monolayer coverage of the adsorbate at the outer surface of the adsorbent. The model assumes uniform energies of adsorption

onto the surface and no transmigration of adsorbate in the plane of the surface. Based upon these assumptions, Langmuir represented the following equation:

$$q_e = q_{max} K_L C_e / 1 + K_L C_e \quad (2)$$

Langmuir adsorption parameters were determined by transforming the Langmuir equation (6) into linear form.

$$C_e/q_e = C_e/q_{max} + 1/(K_L . q_{max}) \quad (3)$$

Where q_e is the amount of dye adsorbed at equilibrium (mg/g), q_{max} is the theoretical maximum monolayer sorption capacity (mg/g), K_L is Langmuir isotherm constant (L/mg) and C_e is the equilibrium concentration of dye in solution (mg L^{-1}). The values of q_{max} and K_L were computed from the slope and intercept of the Langmuir plot of C_e/q_e versus C_e.

For The essential features of the Langmuir adsorption process, the influence of the isotherm shape on whether adsorption is favorable or unfavorable can be classified by a dimensionless separation factor R_L, which is considered as a more reliable indicator of the adsorption capacity. This constant is given by the following [46]:

$$R_L = \frac{1}{1 + K_L C_o} \quad (4)$$

Where C_o is the initial dye concentration and K_L is the Langmuir adsorption constant (L/mg). The values of R_L indicate the shapes of isotherms to be either unfavorable (R_L> 1), linear (R_L= 1), favorable (0 □ R_L□ 1) or irreversible (R_L= 0). Favorable adsorption is reported when the R_L values are between 0 and 1.

3.1.2. Freundlich model

The Freundlich equilibrium isotherm [47] is used for the description of multilayer adsorption with interaction between adsorbed molecules. Model predicts that the dye concentrations on the material will increase as long as there is an increase of the dye concentration in the solution. Usually it applies to adsorption onto heterogeneous surfaces with a uniform energy distribution and reversible adsorption. The application of the Freundlich equation suggests that adsorption energy exponentially decreases on completion of the adsorption centers of an adsorbent. The empirical equation proposed by Freundlich:

$$q_e = K_F C_e^{\frac{1}{n}} \quad (5)$$

Where K_F is Freundlich isotherm constant (mg/g), n is adsorption intensity; Ce is the equilibrium concentration of adsorbate (mg/L), q_e is the amount of metal adsorbed per gram of the adsorbent at equilibrium (mg/g). Linearizing equation is:

$$\ln q_e = \ln K_F + \left(1/n\right) \ln C_e \quad (6)$$

The constant $K_F$is an approximate indicator of adsorption capacity, while 1/n is a function of the strength of adsorption in the adsorption process [48]. If n = 1 then the partition between the two phases are independent of the concentration. If value of 1/n is below one it indicates a normal adsorption. On the other hand, 1/n being above one indicates cooperative adsorption [48].

4. Results and discussion

4.1. X-ray diffraction (XRD)

The XRD patterns of the prepared ZnO samples ZnO, N-ZnO and S-ZnO are shown in Fig 5. The figure shows typical peak patterns at 31.77, 34.43, 36.27, 47.35, 56.61 and 62.83, which correspond to the (100), (002), (101), (102), (110) and (103) planes, respectively. The intense peaks in the XRD pattern of these samples clearly show the formation of the hexagonal Wurtizite structure ZnO (space group: P63mC) as indexed in the standard data (JCPDS Card No. 36-1451, a=3.249 Å and c=5.206 Å) [49]. Even the doped samples present the ZnO crystalline structure, indicating that N or S did not interfere in crystal formation. Main diffraction peaks corresponding to ZnO plane are presented in Fig. 5. No characteristic peaks of impurities and other phases are observed [50, 51]. After the doping process, no modification in diffraction peaks of ZnO lattice was observed, indicating that the nitrogen incorporation in the ZnO lattice or the substitution of $O^{2-}$by N^{3-} or S^{2-} (substitutional N or S) does not modify any crystallographic parameters of ZnO lattice. The preparation through oxalate route and in presence of Tween 80 as structure directing agent and capping agent results in introduce steric hindrance between the particles thereby preventing agglomeration. It was observed that introducing S decrease the crystallinity of ZnO.

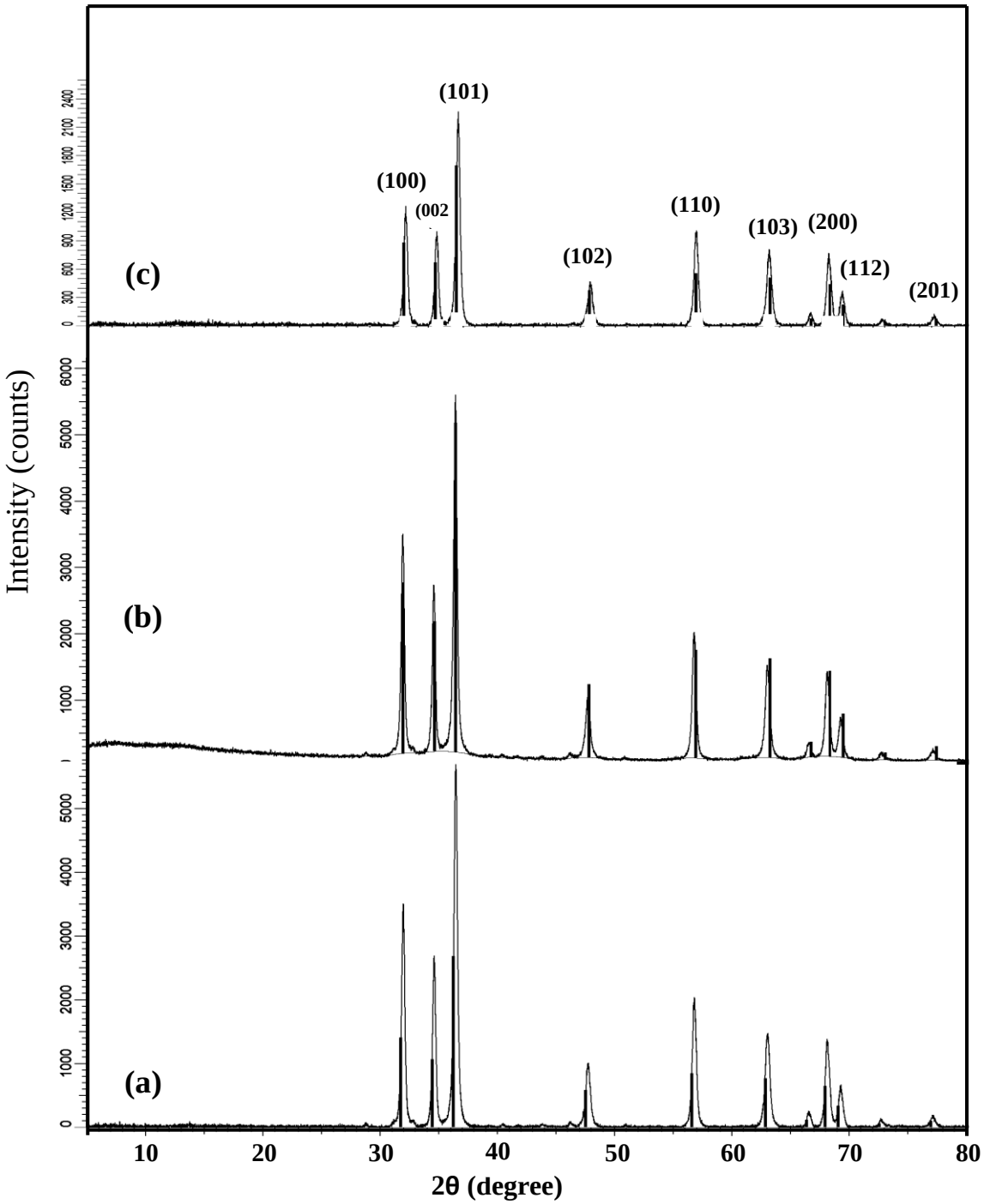

Fig. 5: XRD patterns of a) ZnO b) N-ZnO c) S-ZnO

4.2. Scanning electron microscopy (SEM)

Fig. 6 shows SEM images of the doped and pure powder samples, indicating no significant difference in particle morphology with N or S loading. The predominant morphology of the samples is almost heterogeneous spherical and rectangular nanoparticles in the form of aggregates for almost all samples. The samples have diameters around 31 nm, 21 nm and 26 nm, for ZnO, N-ZnO and S-ZnO, respectively. It was shown that the introducing N or S causing decrease the particle size. The images also show well homogeneity in particles size and shapes.

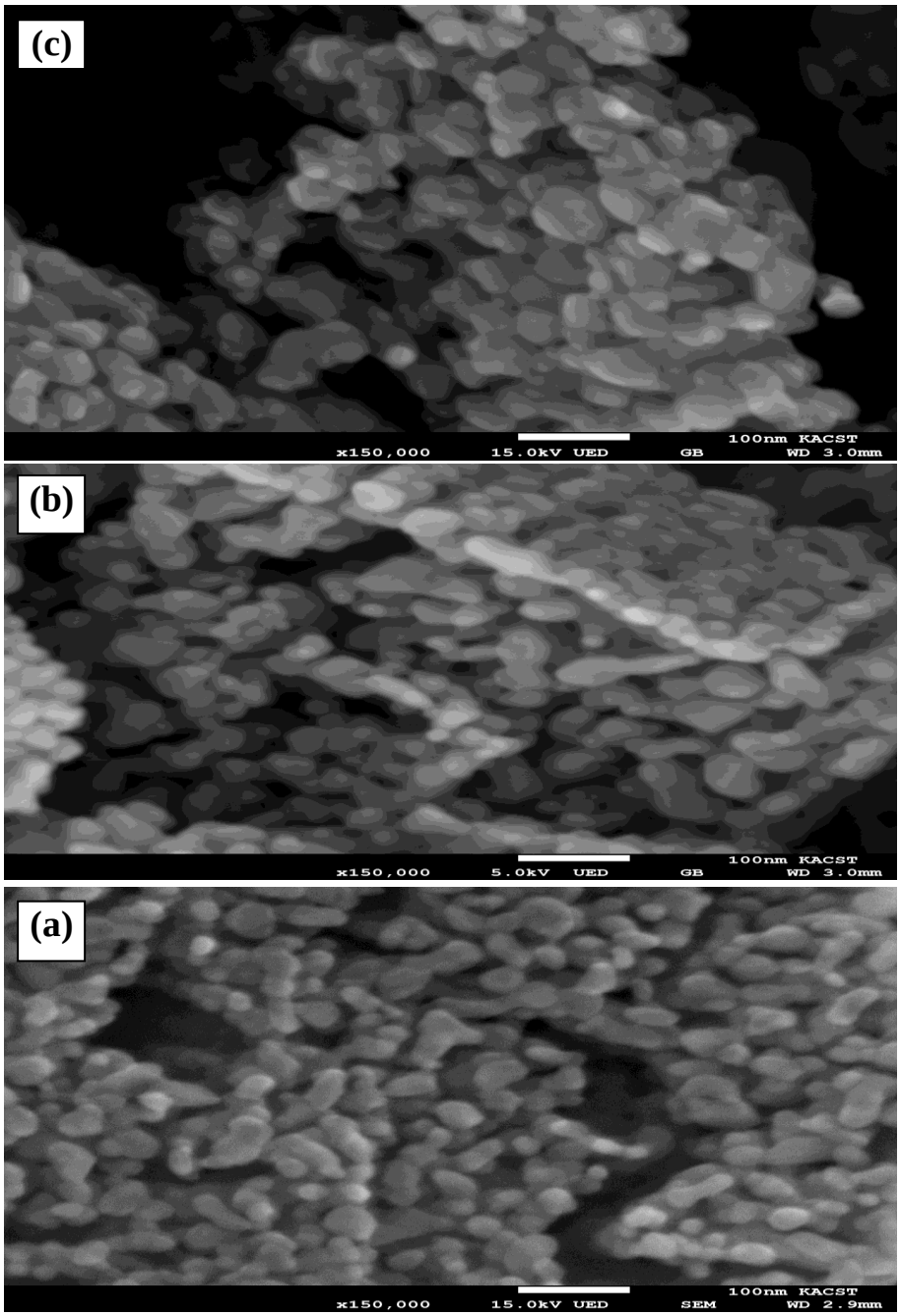

Fig. 6: SEM images of a)ZnO b) N-ZnO c) S-ZnO

4.3. Optical properties

As shown in Fig. 7 the optical absorption spectrum of the studied ZnO samples shows mainly one excitonic peak at wavelength lying in the range of 380 nm which is a characteristic of ZnO.

It was observed that the doped ZnO samples have absorption light range higher than that of pure sample indicating the effect of doping in enhancement of the efficiency of the absorption of visible light.

The maximum absorption wavelengths for the doped samples shifts to higher values with the N or S loading and thus they present visible absorption. The visible absorption is attributed to nitrogen or S incorporation in the crystalline lattice of ZnO [52, 53].

The enhanced absorption of the N-ZnO and S-ZnO samples in the whole visible region can be attributed to the presence of N and S elements. However, the red-shift of absorption edge in comparison with the pure ZnO may suggest a rearrangement of the energy levels of ZnO.

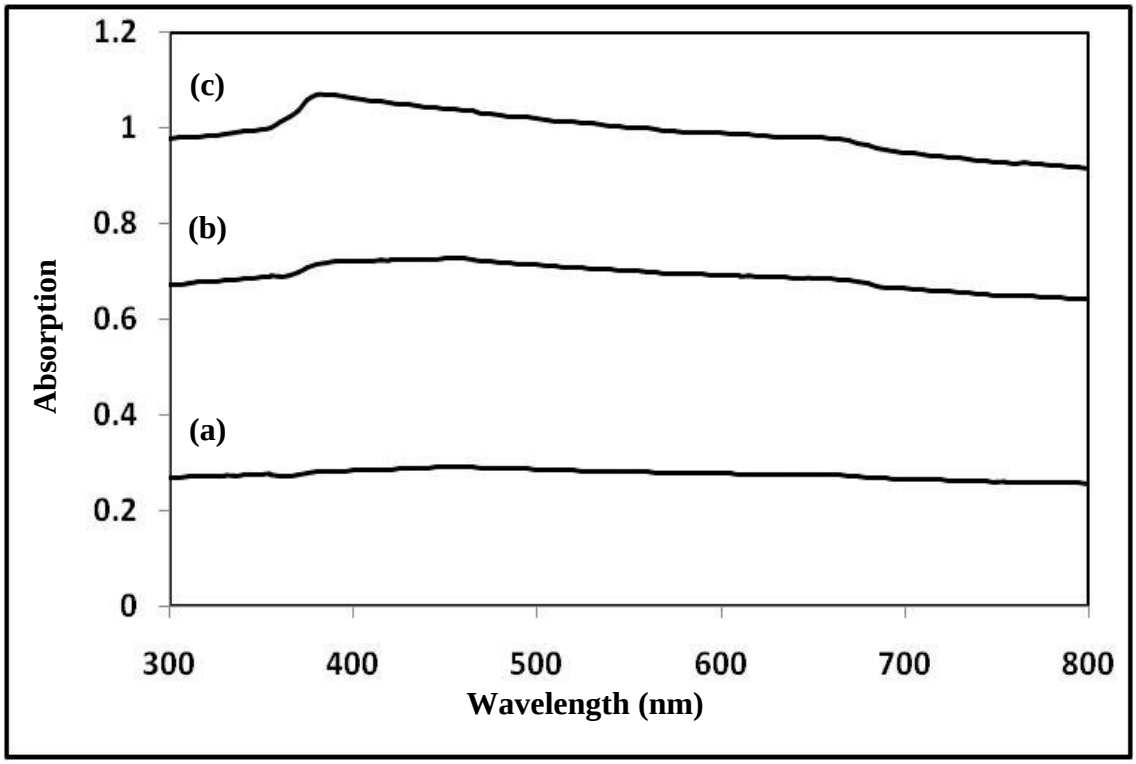

Fig. 7: UV-Vis absorption spectra of: a) ZnO b) N-ZnO c) S-ZnO

4.4. Adsorption

4.4.1. Adsorption studies

The adsorptive removal of MB dye on ZnO, N-ZnO and S-ZnO from aqueous solutions was studied at λ_{max}= 665 nm. Adsorption of dye was occurred at pH 7.0, and 298 K and represented in Fig. 8. The percentage of removal (%R) of dye in the supernatant solution is calculated using the following relation:

$$\%R = \frac{C_0 - C_t}{C_0} \times 100$$

Where C_o (mg/L) is the initial concentration of the dye solution and C_t (mg/L) is the concentration of the dye solution at time t = 55 min. The pure ZnO sample showed the highest adsorption value (66.7 %). On the other hand the doped sample with S give higher adsorption percentage than that of N doped samples as shown in Table 2. This may be attributed to the surface area and porosity as well as the active sites on pure and S doped samples.

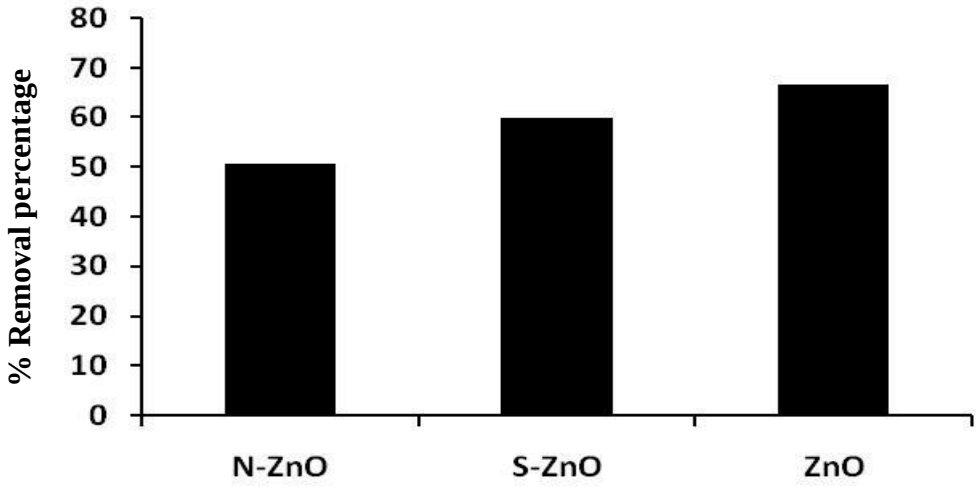

Fig.8: Removal percentage of MB dye on different samples.

Table 2: The adsorption percent and adsorption capacity of MB dye (50 mg/L) on pure and doped ZnO samples at pH 7.0.

Samples	MB dye	
	q_e(mg/g)	Adsorption percent (%)
ZnO	33.35	66.7
S-ZnO	29.93	59.9
N-ZnO	25.35	50.7

4.4.2. Equilibrium adsorption isotherms

The equilibrium of adsorption is one of the critical physicochemical parts of the estimation relationship between the amount of adsorbate per unit of adsorbent (q_e) and its equilibrium solution concentration (C_e) at a constant-temperature and it is known as the adsorption isotherm. There are several isotherm models available for analyzing experimental sorption equilibrium parameters, the most common being the Langmuir and Freundlich models.

The obtained experimental equilibrium adsorption data were analyzed utilizing Langmuir and Freundlich models. The fitting data of these two models are shown in Fig. 9 (a, b).

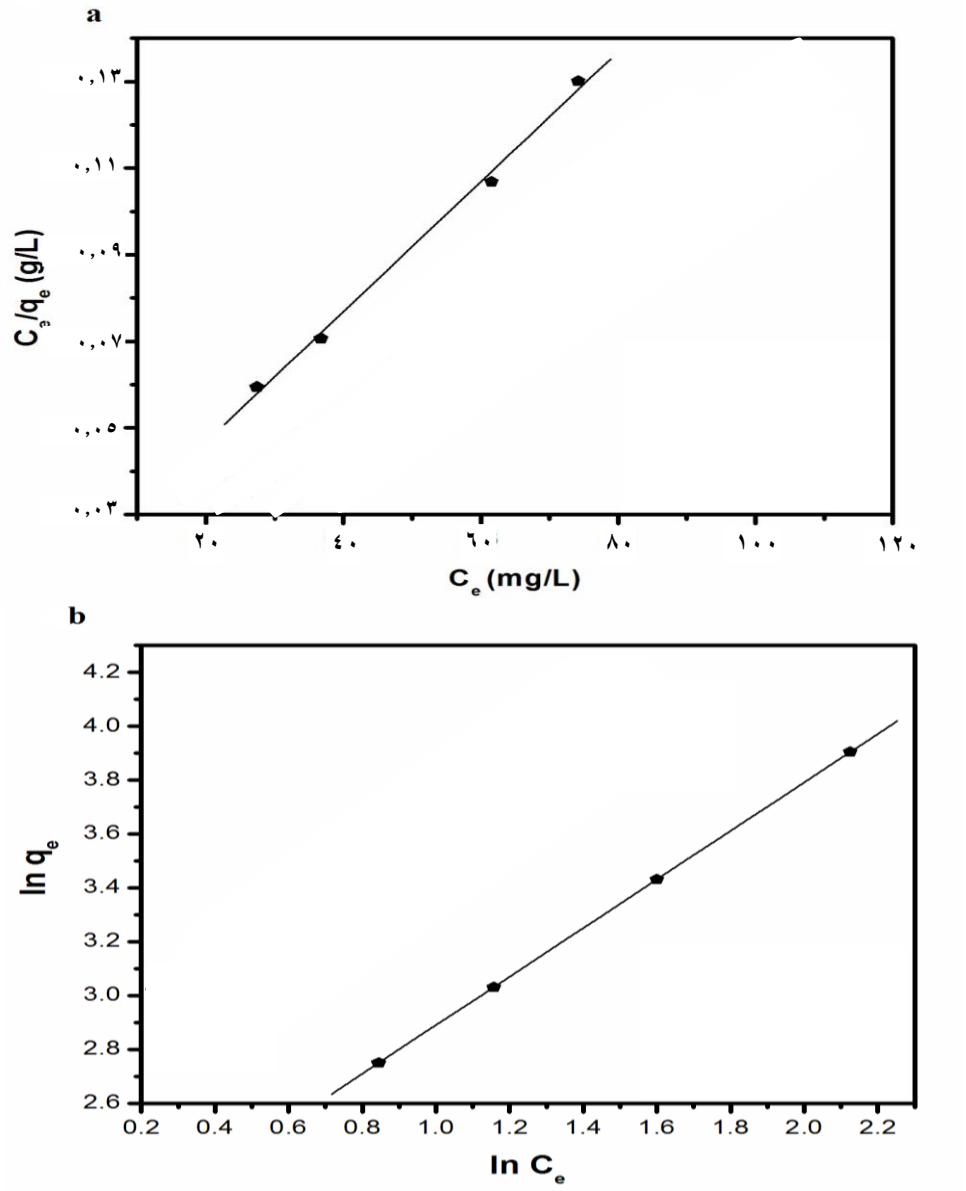

Fig. 9: Linearized adsorption equilibrium isotherms of MB dye by ZnO nanopowder a) Langmuir linear equation b) Freundlich linear equation

The evaluated Langmuir and Freundlich isothermal parameters for the adsorption of dye on as-prepared pure ZnO nanoparticles (highest removal percentage) are given in Table 3. As shown in Table 3, the Langmuir and Freundlich isotherms are found to be straight over the whole concentration range studied with R^2 > 0.99. Considering the high values of the regression coefficient R^2 near unity in this table, it is clear that Freundlich model fits better adsorption equilibrium data in case of MB dye adsorption. In addition, the values of 1/n □1 indicated that the adsorption of the dye is favourable by Freundlich isotherm model (Table 3). It can also be observed that the values of q_{max} are lower than $q_{e(exp)}$, which confirmed the unfavourable uptake of the dye process by Langmuir isotherm model. Accordingly, the experimental equilibrium data can be better described by Freundlich isotherm model demonstrating positive cooperativity in binding and a heterogeneous nature of adsorption.

Table ٣. Langmuir and Freundlich isotherm constants for MB dye adsorption onto pure ZnO nanoparticles.

Sample	**Langmuir isotherm model**				**Freundlich isotherm model**			
	q_{max} (mg/g)	**K_L (L/mg)**	**R^2**	**R_L**	**K_F (mg/g)**	**n**	**1/n**	**R^2**
ZnO	**18.9**	**4.8**	**0.992**	**0.29**	**7.3**	**1.11**	**0.90**	**0.999**

5. Conclusions

Nano-crystalline ZnO, N and S doped ZnO particles were synthesized using template method with particle diameter ranged from 21 to 31 nm. The samples well characterized with different techniques. The doping process enhanced the absorption of visible light. Moreover, the equilibrium data of adsorption are in good agreement with the Freundlich isotherm model. The samples show effective adsorption at short time 55 min.

Refrences

[1] R. H. J. Hannink and A. J. Hill, Nanostructure control of materials, Woodhead Publishing Limited and CRC Press LLC, Cambridge England (2006) and references there in.

[2] M. Haruta, Catal. Today, 36 (1997) 153.

[3] Gerbericha and W. *et al*., *J.* Mech. and Phys. of Soli., 51 (2003) 979.

[4] M. Verdier, M. Niewczas, J. D. Embury, M. Nastasi and H. Kung, Mat. Resear. Soc. Sym. Proc., 77 (1998) 522.

[5] W. P. Kirk and M. A. Reed, Nanostructures and Mesoscopic Systems, New York, Academic Press, 1992.

[6] H. M. Huang, X. M. Xiao and B. Yan, Wat. Sci. Technol., 59 (2009) 1093.

[7] R. Rounds, "Azo Dyes." in Encyclopedia of Chemical Technology, A. Standen, Ed., Vol. 6, 2nd ed., New York, Interscience Publishers, a division of John Wiley & Sons, Inc. (1963) 401.

[8] D. J. Sarokin, W. R. Muir, C. G. Miller and S. R. Sperber, Cutting Chemical Wastes. New York: Inform, Inc. (1985).

[9] G. M. Shaul, C. R. Dempsey and K .A. Dostal. "Fate of Water Soluble Azo Dyes in the Activated Sludge Process." EPA/600/ S2-88/ 030, Water Engineering Research Lab. Cincinnati, OH, (1988).

[10] M. d. Bethesda, "Carcinogenicity of Azo Dyes, Aryl Amines, and Related Compounds." Dept. of Health, Education and Welfare, Public Health Service, National Institutes of Health, National Cancer Institute Spdngiield, Va. (1985).

[11] H. Shu and C. Huang, Hazardous Substance Management Research Center, Department of Chemical Engineering, Chemistry and Environmental Science, New Jersey Institute of Technology, Newark, New Jersey 07102, U.S.A.

[12] A. Kumbhar and G. Chumanov, J. Nanopart. Res. 7 (2005) 489.

[13] A. R. Cestri, E. F. S. Vieira, A. A. Pinto and E. C. N. Lopes, J. Colloid Interf. Sci.,292 (2005) 363.

[14] A. Krysztafkiewicz, S. Binkowski and T. Jesionowski, Appl. Surf. Sci., 199 (2002) 31.

[15] K. C. Chen, J. Y. Wu, C. C. Huang, Y. M. Liang and S. C. J. Hwang, J. Biotech., 101 (2003) 241.

[16] T. Robinson, G. McMullan, R. Marchant and P. Nigam, Biosour. Technol., 77

(2001) 247.
[17] T. Jesionowski, Dyes and Pigments, 55 (2002) 133.
[18] E. Eren and B. Afsin, Dyes and Pigments, 76 (2008) 220.
[19] A. R. Cestari, E. F. S. Vieira, G. S. Vieira and L. E. Almeida, J. Hazard. Mater. B,138 (2006) 133.
[20] Y. C. Sharma, S. N. Uma and G. F. Upadhyay, J. Appl. Sci. Enviro. Sanit.,4 (2009) 21.
[21] A. Khenifi , Z. Bouberka, F. Sekrane, M. Kameche and Z. Derriche, Adsorption, 13 (2007) 149.
[22] R. C. Torane, K. S. Mundhe, A. A. Bhave, G. S. Kamble, R. V. Kashalkar and N. R. Deshpande, Der. Pharma.Chemica.,2 (2010) 171.
[23] D. Bingola, S. Veli, S. Zora and U. Ozdemirb, Synth. Met., 162 (2012) 1566.
[24] S. C. Kuiry, S. Patil, S. Deshpande and S Seal, J. Phys. Chem. B, 109 (2005) 6936.
[25] J. E. Jaffe, R. Pandey, and A. B. Kunz, Phys. Rev. B 43 (1991)14030
[26] M. H. Huang, Y. Wu, H. Feick, N. Tran, E. Weber and P. D. Yang, Adv. Mater., 13 (2001) 113.
[27] K. Ghule, A. V. Ghule, B. Chen and Y. Ling, Green Chem.,8 (2006) 1034
[28] Z.X. Dai, A. Nurbawono, A.H. Zhang, M. Zhou, Y.P. Feng, G.W. Ho, C. Zhang, J. Chem. Phys. 134 (2011) 104706.
[29] F.X. Wang, L. Liang, L. Shi, M.S. Liu, J.M. Sun, Dalton Trans. 43 (2014) 16441.
[30] H.W. Bai, Z.Y. Liu, D.D. Sun, Chem. Asian J. 7 (2012) 1772.
[31] Y.C. Qiu, K.Y. Yan, H. Deng, S.H. Yang, Nano Lett. 12 (2012) 407.
[32] M. Debbichi, T. Sakhraoui, L. Debbichi, M. Said, J. Alloys Comp. 578 (2013) 602.
[33] J.M. Coronado, F. Fresno, M.D. Hernández-Alonso, R. Portela, Design of Advanced Photocatalytic Materials for Energy and Environmental Applications, Springer, New York, 2013
[34] X. Chen, S. Shen, L. Guo, S.S. Mao, Chem. Rev. 110 (2010) 6503.
[35] S.M. Lam, J.C. Sin, A.Z. Abdullah, A.R. Mohamed, Desalin. Water Treat. 41 (2012) 131.
[36] S.Y. Bae, H.W. Seo, J. Park, J. Phys. Chem. B 108 (2004) 5206.
[37] Z. Li, S. Sun, X. Xu, B. Zheng, A. Meng, Catal. Commun. 12(2011) 890.

[38] X. Zong, C. Sun, H. Yu, Z.G. Chen, Z. Xing, D. Ye, G.Q. Lu, X. Li, L.Wang, J. Phys. Chem. C 117 (2013) 4937.

[39] Z. Yu, L.C. Yin, Y. Xie, G. Liu, X. Ma, H.M. Cheng, J. Colloid Interface Sci. 400 (2013) 18.

[40] C. Di Valentin, G. Pacchioni, Acc. Chem. Res. 47 (2014) 3233.

[41] F. Gallino, C. Di Valentin, G. Pacchioni, M. Chiesa, E. Giamello, J. Mater. Chem. 20 (2010) 689.

[42] A. B. Patil, K. R. Patil, S. K. Pardeshi, J. Hazard. Mater., 183 (2010) 315.

[43] X. Xie, P. Zhan, L. Li, D. Zhou, D. Guo, J. Meng, Y. Bai, W.Zheng, J. Alloys Comp. 644 (2015) 383.

[44] A. B. Patil, K. R.Patil, S. K. Pardeshi, J. Solid State Chem., 184 (2011) 3273.

[45] I. Langmuir, Journal of the American Chemical Society 40 (1918) 1361.

[46] T. W. Weber, R. K. Chakravorti, J. Amer. Inst. Chem. Engin., 20 (1974) 228.

[47] H. M. F. Freundlich, J. Phys. Chem., 57 (1906) 385..

[48] H. Zhang, Y. Tang, D. Cai, X. Liu, X. Wang, Q. Huang and Z. Yu, J. Hazard. Mater., 181 (2010) 801.

[49] J. Liu, X. Huang, J. Duan, H. Ai, P. Tu, Mater. Lett. 59 (2005) 3710.

[50] A. Meng, X. Li, X. Wang, Z. Li, Preparation, Ceram. Int. 40 (2014)9303.

[51] N.R. Yogamalar, M. Ashok, A.C. Bose, Funct. Mater. Lett. 4 (2011) 271.

[52] B. Liu, X. Zhao, L. Wen, Mater. Sci. Eng. B 134 (2006) 27.

[53] X. Li, B. Keyes, S. Asher, S.B. Zhang, S.H. Wei, T.J. Coutts, S. Limpijumnong,C.G.V. de Walle, Appl. Phys. Lett. 86 (2005) 122107.